Eur. Phys. J. B (2014) 87: 22
DOI: 10.1140/epjb/e2013-40842-3

THE EUROPEAN PHYSICAL JOURNAL B

Regular Article

Splitting of satellites in a time-dependent Kondo model

Thanh Thi Kim Nguyen[1,2,a] and Minh-Tien Tran[2]

[1] Department of Physics, University of Cincinnati, Cincinnati, 45221 Ohio, USA
[2] Institute of Physics, Vietnam Academy of Science and Technology, 10 Dao Tan, Hanoi, Vietnam

Received 17 September 2013 / Received in final form 20 November 2013
Published online 27 January 2014 – © EDP Sciences, Società Italiana di Fisica, Springer-Verlag 2014

Abstract. A time-dependent Kondo model, where both the voltage and the Kondo couplings oscillate on time, is considered. The bosonization technique at the Toulouse limit is applied to study the conductance and the magnetic susceptibility. It is shown that in addition to the satellites of the Kondo peak that appear in the conductance and the susceptibility as a function of the magnetic field or dc voltage, when the voltage oscillates, these satellites further split when the Kondo couplings also oscillate on time. The distance of the satellite splitting solely depends on the ratio between the oscillation frequencies of the voltage and of the Kondo couplings. When the Kondo couplings oscillate more rapidly than the voltage, the distance of the satellite peaks can be smaller than the voltage oscillation frequency.

1 Introduction

The Kondo effect is one of the central topics in condensed matter physics, and has attracted attention for nearly a half century [1,2]. The effect stems from a macroscopic quantum coherent coupling between a localized magnetic moment and a Fermi sea of electrons. The local magnetic moment is screened by hybridization with the itinerant electron spins, leading to the formation of a bound spin-singlet state. The Kondo effect has been used to explain successfully many extraordinary properties of dilute magnetic alloys and heavy fermion materials [2]. With the developments of mesoscopic physics and nano-technology, the Kondo effect again lies in the heart of physical properties of quantum dot devices, where the dots play as Kondo-like impurities [3–13]. The transport and magnetic properties of quantum dots (QD) exhibit the Kondo effect features [12,13]. In equilibrium, the Kondo resonance appears at the Fermi energy in the density of states (DOS) of a QD coupling with two leads, that strongly influences the tunneling conductance of the system at low temperatures. When the source-drain voltage and magnetic field are switched on, they suppress the Kondo peak in the tunneling conductance as function of the source-drain voltage, and split it into two peaks [9–15]. When the voltage varies with time, the Kondo effect in the quantum dot dramatically changes. In non-equilibrium the time-dependent external parameters (namely, source-drain voltage or/and gate voltage) compete with the Kondo singlet correlations that results in a non-trivial dynamics with novel and beyond equilibrium features [16–26]. An ac voltage produces satellite peaks in the tunneling conductance as a function of dc source-drain voltage thanks to the Tien-Gordon theory [27]. The non-equilibrium Kondo effect has attracted a lot attention. Due to the complexity of out-of-equilibrium many-body systems, it is instructive to investigate those cases where the exact non-perturbative solutions are accessible. One particular interesting case is the Kondo model at the Toulouse limit where it becomes exactly solvable [28]. The Toulouse limit displays many generic and universal properties of the strong coupling limit of the Kondo model both in equilibrium [29] and out of equilibrium [14,15,18,30–32]. The previous studies investigated the non-equilibrium Kondo effect in QD resulted from the time dependence either of the voltage bias [14,15,18] or of Kondo couplings [30–32]. When both the voltage and the Kondo couplings vary with time, the non-equilibrium Kondo effect remains open.

In the present paper, we consider a time-dependent Kondo model at the Toulouse limit where both the voltage and the Kondo couplings oscillate on time. We solve the problem non-perturbatively by averaging non-equilibrium Green's functions in the period of the slow oscillation. The differential conductance and the magnetic susceptibility are computed. It is found that the Kondo satellites which appear due to the oscillation of the source-drain voltage are further split due to the effect of the oscillation of the Kondo couplings. The peak splitting distance depends on the ratio between the voltage's frequency and the frequency of the Kondo couplings.

The present paper is organized as follows. In Section 2, the time-dependent Kondo model at the Toulouse limit is introduced. We also present its mapping onto a quadratic effective Hamiltonian in this section. The non-equilibrium Green's function method used to calculate the differential conductance and the magnetic susceptibility is presented

[a] e-mail: nkthanh@iop.vast.ac.vn

in Section 3. The differential conductance and the magnetic susceptibility are derived in Section 4, whereas their numerical calculations and discussions are presented in Section 5. Finally, in Section 6 we present the conclusion.

2 Ac time-dependent Kondo model

2.1 The model at the Toulouse limit

We propose a time-dependent Kondo model based on modeling of a QD coupling with two non-interacting leads of spin-1/2 electrons, each subjects to a separate time-dependent voltage. The coupling of the QD with the leads is modeled through the exchange interactions between the dot and lead spins. Without loss of generality, we assume that the leads are one dimensional, and the dot is placed at the origin. The Hamiltonian of the proposed harmonic time-dependent Kondo model reads

$$\begin{aligned}\mathcal{H} = & iv_F \sum_{\alpha=L,R,\sigma=\uparrow,\downarrow} \int_{-\infty}^{\infty} dx \psi^{\dagger}_{\alpha\sigma} \frac{\partial}{\partial x} \psi_{\alpha\sigma}, \\ & + \frac{V(t)}{2} \sum_{\sigma=\uparrow,\downarrow} \int_{-\infty}^{\infty} dx \left[\psi^{\dagger}_{L\sigma} \psi_{L\sigma} - \psi^{\dagger}_{R\sigma} \psi_{R\sigma} \right] \\ & + \sum_{\alpha,\beta=L,R} \sum_{\lambda=x,y,z} J^{\alpha\beta}_{\lambda}(t) s^{\lambda}_{\alpha\beta} \tau^{\lambda} - H\tau^{z}, \end{aligned} \tag{1}$$

where $\psi^{\dagger}_{\alpha\sigma}(x)$ is the one-dimensional field describing the conduction electrons with spin σ in lead α, labeled right (R) and left (L). The dispersion relation of the lead electrons is linearized around the Fermi level with the Fermi velocity v_F. $V(t) = V_{dc} + V_{ac}\cos(\Omega t)$ is the time-dependent voltage bias applied to the leads across the dot junction. The constant part V_{dc} can be considered as a dc voltage, while V_{ac} is the amplitude of an ac voltage oscillating on time with frequency Ω. The dc part V_{dc} fixes a chemical-potential difference between the two Fermi seas of the leads in relation with the Fermi energy $E_F = 0$. H is the external magnetic field acting on the dot, the spin of which is represented by the Pauli matrices τ^{λ}, ($\lambda = x, y, z$). $J^{\alpha\beta}_{\lambda}(t)$ is the time-dependent of the exchange coupling between the dot and lead electron spins. The spin of the lead electrons is presented as $s^{\lambda}_{\alpha\beta} = \frac{1}{2}\sum_{\sigma\sigma'} \psi^{\dagger}_{\alpha\sigma}(0)\sigma^{\lambda}_{\sigma\sigma'}\psi_{\beta\sigma'}(0)$. Here we also use the natural units with $\hbar = k_B = e = \mu_B = g_i = 1$.

In general, we consider the time-dependence of the Kondo couplings in the form of ac oscillations

$$J^{\alpha\beta}_{\lambda}(t) = J^{\alpha\beta}_{\lambda 0} + J^{\alpha\beta}_{\lambda 1}\cos(\Omega_1 t + \phi_{\alpha\beta}), \tag{2}$$

where $J^{\alpha\beta}_{\lambda 0}$ is the time-independent part of the couplings, and $J^{\alpha\beta}_{\lambda 1}$ is the amplitude of the oscillations with frequency Ω_1. $\phi_{\alpha\beta}$ is the set-off phase of the coupling oscillations. The Kondo couplings can be generated from the Anderson model of the QD with energy level E_d, and large on-site interaction U in the Kondo regime, where both ionization and electron addition energy are much bigger than the tunneling rates: $E_d, U - E_d \gg \Gamma_{L/R}$, and the applied fields do not drive the dot out of this regime: eV_{dc}, eV_{dot}, eV_{ac}, H, Ω, $\Omega_1 < E_d, U - E_d$. In equilibrium they are obtained as a result of the Schrieffer-Wolff transformation [33]. When ionization energy level of the dot varies with time, the time-dependent Schrieffer-Wolff transformation leads the Kondo couplings to be time dependent [19,20,23,24]. In particular, when the energy level E_d oscillates on time between two different values E_{d1} and E_{d2} with $|E_{d2} - E_F| \gg |E_{d1} - E_F|$ and $|E_{d2} - E_{d1}| = 2eV_{dot}$, where for each energy E_{d1} and E_{d2} the quantum dot is assumed to be still in the Kondo regime, the Kondo coupling $J^{\alpha\beta}_{\lambda}(t)$ thus oscillates on time [23,24]. In general, the oscillation frequency of the Kondo couplings is different from the frequency of the applied voltage and of the energy level. We assume that the Kondo couplings are monochromatic oscillations with frequency $\Omega_1 = \Omega/p$, where p is a integer number. It means that the voltage is a harmonic of the Kondo couplings.

In order to extract the exact solution, we consider the Toulouse limit, where the transfer exchange couplings are time independent, and vanish for the transfer exchanges between different leads [15,18,29]

$$J^{LR}_{z} = J^{RL}_{z} = 0,\ J^{LL}_{z} = J^{RR}_{z} = J_z = 2\pi v_F. \tag{3}$$

This set of model parameters is expected to describe well the scaling regime of the Kondo effect even out of equilibrium [15,18]. The scaling trajectories flow to the Toulouse point if $J^{LL}_{\perp 0} = J^{RR}_{\perp 0}$, $J^{RL}_{\perp 0} = 0$, in which the two leads are decoupled, the channels are just the right and left leads, which carry no current [15]. The time dependent oscillations of the perpendicular couplings are turned on adiabatically

$$\begin{aligned} J^{RL}_{\perp}(t) &= J^{LR}_{\perp}(t) = J^{RL}_{\perp}\cos(\Omega_1 t), \\ J^{LL}_{\perp}(t) &= J^{LL}_{\perp 0} + J^{LL}_{\perp}\cos(\Omega_1 t), \\ J^{RR}_{\perp}(t) &= J^{LL}_{\perp 0} + J^{RR}_{\perp}\cos(\Omega_1 t). \end{aligned} \tag{4}$$

Here, the time independent $J^{RL}_{\perp 0}$ has been omitted, since we want to consider the case, when the time dependent parts are absent, the two leads are completely decoupled and no current tunnels through the dot, as just discussed above. The finite value of $J^{RL}_{\perp 0}$ couples the two leads even in equilibrium, and the situation becomes complicated when the time dependent parts of the coupling are switched on. In equation (4) we also omit the phase set-off $\phi_{\alpha\beta}$ for simplicity. The anisotropic Kondo Hamiltonian at the Toulouse limit has well explained many universal features of the equilibrium Kondo physics in QD [29]. It is expected to correctly describe the strong-coupling regime of the non-equilibrium Kondo effect. Indeed, previous studies of the model with the dc [14,15] and ac [18] voltage bias have shown all the qualitative features of Kondo-assisted tunneling: a zero-bias anomaly that splits in an applied magnetic field; Fermi-liquid characteristics in the low-T and low-V differential conductance; satellites in the differential conductance at $eV = \pm n\Omega$, for an ac voltage with frequency Ω. Recently, this model has also been adopted

to study the problems of the interaction quench [30] and the periodically switched on and off Kondo couplings [32].

The aim of the present work is to study the non-equilibrium Kondo effect when the voltage $V(t)$ is a harmonic of the monochromatic oscillations of the Kondo couplings $J_\perp^{\alpha\beta}(t)$, i.e., $\Omega_1 = \Omega/p$, $p \in \mathbb{N}$. In order to neglect the charge fluctuations on the dot caused by hopping processes between the central region and the conductance band by absorbing or emitting quanta of the driving frequency, the frequencies of the applied fields have to be small enough, i.e., $\Omega,\ \Omega_1 \ll |E_d|, |U - E_d|$.

2.2 Mapping onto a solvable model

In order to map the introduced non-equilibrium Kondo model at the Toulouse limit into a solvable model we first bosonize the Hamiltonian (1)

$$\psi_{\alpha\sigma}(x) = F_{\alpha\sigma} \exp(-i\Phi_{\alpha\sigma}(x))/\sqrt{2\pi a},$$

where $\Phi_{\alpha\sigma}(x) = \sqrt{\pi}\Big[\int_{-\infty}^{x} dx' \Pi_{\alpha\sigma}(x') - \phi_{\alpha\sigma}(x)\Big]$. Here $F_{\alpha\sigma}$ is the Klein factors, and $\phi_{\alpha\sigma}(x)$ are Bose fields and $\Pi_{\alpha\sigma}(x)$ are their conjugate momenta, satisfying commutation relations[1]. Next, we introduce new bosonic fields: charge $\phi_c(x)$, pseudo-spin $\phi_s(x)$, flavor $\phi_f(x)$, and pseudo-flavor $\phi_{sf}(x)$ as $\phi_c(x) = \sum_{\alpha,\sigma} \phi_{\alpha\sigma}/2$, $\phi_s(x) = \sum_{\alpha,\sigma} \sigma^z_{\sigma\sigma}\phi_{\alpha\sigma}/2$, $\phi_f(x) = \sum_{\alpha,\sigma} \sigma^z_{\alpha\alpha}\phi_{\alpha\sigma}/2$, $\phi_{sf}(x) = \sum_{\alpha,\sigma} \sigma^z_{\alpha\alpha}\sigma^z_{\sigma\sigma}\phi_{\alpha\sigma}/2$, and also for Π_ν, Φ_ν, N_ν, $\nu = c, s, f, sf$. Then we perform the transformation of the Hamiltonian $\mathcal{U}\mathcal{H}\mathcal{U}^{-1}$ with $\mathcal{U} = \exp[-i\tau^z\Phi_s(0)]$. Four more Klein factors F_ν are introduced, which satisfy $[F_\nu, N_{\nu'}] = \delta_{\nu\nu'}F_\nu$ and relate to the old ones as $F^\dagger_{L\downarrow}F_{L\uparrow} = F_sF_{sf}$, $F^\dagger_{R\downarrow}F_{R\uparrow} = F_sF^\dagger_{sf}$, $F^\dagger_{R\downarrow}F_{L\uparrow} = F_fF_s$, $F^\dagger_{R\uparrow}F_{L\downarrow} = F_fF^\dagger_s$. The new impurity fermion is thus represented as $d^\dagger = F_s\tau^+$, $d = F^\dagger_s\tau^-$, $\tau^z = d^\dagger d - 1/2$. We now re-fermionize these bosonic fields as $\Psi_m(x) = F_m \exp(-i\Phi_m(x))/\sqrt{2\pi a}$ to re-write the Hamiltonian in which all the charge, spin, flavor, and spin flavor degrees of freedom are separated

$$\begin{aligned}
\mathcal{H}' = {} & iv_F \sum_{\nu=c,s,f,sf} \int_{-\infty}^{\infty} dx \psi^\dagger_\nu(x)\partial_x\psi_\nu(x) \\
& + \left[H - (J_z - 2\pi v_F) : \psi^\dagger_s(0)\psi_s(0) :\right](d^\dagger d - 1/2) \\
& + \int_{-\infty}^{\infty} dx\ [V_{dc} + V_{ac}\cos(\Omega t)]\, \psi^\dagger_f(x)\psi_f(x) \\
& + \frac{J_t(t)}{2\sqrt{2\pi a}}\Big[\Psi^\dagger_f(0) - \Psi_f(0)\Big](d + d^\dagger) \\
& + \frac{J_a(t)}{2\sqrt{2\pi a}}\Big[\Psi^\dagger_{sf}(0) - \Psi_{sf}(0)\Big](d + d^\dagger) \\
& + \frac{J_s(t)}{2\sqrt{2\pi a}}\Big[\Psi^\dagger_{sf}(0) + \Psi_{sf}(0)\Big](d^\dagger - d), \qquad (5)
\end{aligned}$$

where $: \psi^\dagger_s(0)\psi_s(0) :$ means normal ordering with respect to the unperturbed ψ_s Fermi sea. Here we have also defined

$$\begin{aligned}
J_t(t) &= J^{LR}_\perp(t) = J^{RL}_\perp \cos(\Omega_1 t), \\
J_s(t) &= (J^{LL}_{\perp 0} + J^{RR}_{\perp 0})/2 + (J^{LL}_\perp + J^{RR}_\perp)\cos(\Omega_1 t)/2, \\
J_a(t) &= (J^{LL}_\perp - J^{RR}_\perp)\cos(\Omega_1 t)/2.
\end{aligned}$$

From our assumption in equation (3), $J_z = 2\pi v_F$, we are in the Emery-Kivelson line [29], the Hamiltonian (5) reduces to quadratic form, which is exactly solvable in equilibrium [29] and out of equilibrium [15,18]. The charge and spin sectors are decoupled from the local flavor and spin flavor, reduced to a collection of uncoupled harmonic oscillators. Therefore, they will be omitted from now on. Finally, by introducing Majorana fermions $\hat{a} = (d^\dagger + d)/\sqrt{2}$ and $\hat{b} = (d^\dagger - d)/i\sqrt{2}$, one arrives at the following Hamiltonian

$$\begin{aligned}
\mathcal{H} = \sum_k \Big[& \varepsilon_{fk}(t)c^\dagger_{fk}c_{fk} + \varepsilon_{sfk}c^\dagger_{sfk}c_{sfk} \\
& - iH\hat{a}\hat{b} + \frac{J_t(t)}{2\sqrt{\pi a}}(c^\dagger_{fk} - c_{fk})\hat{a} \\
& + \frac{iJ_s(t)}{2\sqrt{\pi a}}(c^\dagger_{sfk} + c_{sfk})\hat{b} + \frac{J_a(t)}{2\sqrt{\pi a}}(c^\dagger_{sfk} - c_{sfk})\hat{a}\Big], \qquad (6)
\end{aligned}$$

where $\varepsilon_{fk}(t) = 2\pi v_F k + e[V_{dc} + V_{ac}\cos(\Omega t)]$, $\varepsilon_{sfk} = 2\pi v_F k$, c_{jk} is the Fourier image of $\psi_j(0)$ in the momentum space. Here after we will work with Hamiltonian (6) to calculate physical observables.

3 Average Green's functions

It is well known that the Keldysh Green's function technique is an efficient method for treating non-equilibrium systems[2]. This technique has been applied to determine the fully nonlinear, time dependent current through interacting and non-interacting resonant tunneling systems [36]. However, the complete result was only obtained for the time independent level-width function (or tunneling amplitude). Similarly, the Hamiltonian in equation (6) has been solved exactly only when the couplings are constant [18]. Later, the steady state in the Kondo model at the Toulouse limit, in which the couplings are periodically switched on and off, has been investigated by analyzing exact analytical results for the local spin dynamics at zero temperature [32]. The exact solution for the time dependent Hamiltonian in equation (6) still remains open. In this section, we present an average non-equilibrium Green's function method which gives good results in the high enough frequency regime.

[1] The detailed bosonization technique can be found in text books and review articles, for instance [34].

[2] The Keldysh Green's function technique can be found in several text books as well as review articles, we show here one book, in which we follow the detail technique [35].

3.1 Non-interacting Green's functions of flavor fermions

The non-interacting Green's function of the flavor fermion, which is defined as:

$$g_{fk}(t,t') = -i\left\langle T_K\left\{c_{fk}(t)\, c_{fk}^{\dagger}(t')\right\}\right\rangle, \tag{7}$$

can be represented through its retarded, advanced, and Keldysh components

$$\begin{aligned} g_{fk}^{R,A}(t,t') &= \mp i\Theta(\pm t \mp t') e^{-i2\pi v_F k\left(t-t'\right)} \\ &\quad \times e^{-i\frac{V_{ac}}{\Omega}\left[\sin(\Omega t)-\sin\left(\Omega t'\right)\right]}, \\ g_{fk}^{K}(t,t') &= i\left[2f\left(2\pi v_F k + V_{dc}\right) - 1\right] e^{-i2\pi v_F k\left(t-t'\right)} \\ &\quad \times e^{-i\frac{V_{ac}}{\Omega}\left[\sin(\Omega t)-\sin\left(\Omega t'\right)\right]}, \end{aligned} \tag{8}$$

where $f(x) = 1/(\exp(x/T)+1)$ is the Fermi distribution function at temperature T. We set the chemical potential of the spin flavor lead as the reference of the energy level. When the oscillation voltage is applied, the chemical potential additionally acquires the voltage, and it oscillates on time with amplitude V_{ac} around the fixed value V_{dc}. Using the identity $\exp[x(a-1/a)/2] = \sum_{n=-\infty}^{\infty} a^n J_n(x)$, where $J_n(x)$ are the integer Bessel functions of the first kind, and changing variables

$$\begin{aligned} \tau &= t - t', \\ T &= \frac{t+t'}{2}, \end{aligned} \tag{9}$$

we find

$$\begin{aligned} g_{fk}^{R,A}(\tau,T) &= \mp i\Theta(\pm\tau) \sum_{m,n=-\infty}^{\infty} J_n\left(\frac{V_{ac}}{\Omega}\right) J_m\left(\frac{V_{ac}}{\Omega}\right) \\ &\quad \times e^{-i[\varepsilon_k + (n+m)\Omega/2]\tau} e^{-i\Omega(n-m)T}. \end{aligned} \tag{10}$$

Because the flavor fermion chemical potential oscillates on time with frequency Ω, one can take the average of the non-interacting Green's function over time $T \gg \Omega^{-1}$ [37]. The Fourier transform regarding the time difference τ of the average Green's function thus remains as in equilibrium [27]

$$\overline{g_f^{R,A}(\omega)} = \sum_k \overline{g_{fk}^{R,A}(\omega)} = \mp\frac{i}{2v_F}. \tag{11}$$

Here the linearization for the energy spectrum around the Fermi level has been applied [34]. However, the effect of oscilation voltage $V_{ac}(t)$ modifies the Keldysh component $g_{fk}^{K}(t,t')$. We obtain the average of the Keldysh component $\overline{g_f^K(\omega)}$ in the Fourier space corresponding the time difference τ as:

$$\begin{aligned} \overline{g_f^K(\omega)} &= \sum_k \overline{g_{fk}^K(\omega)} \\ &= \frac{i}{v_F}\sum_n J_n^2\left(\frac{V_{ac}}{\Omega}\right)\left[2f\left(\omega - n\Omega + V_{dc}\right) - 1\right]. \end{aligned} \tag{12}$$

Once the retarded, advanced and Keldysh Green's functions are determined, the Green's functions of a combination of the flavor fermions can be calculated too. For example, the following non-interacting Green's function can be calculated without difficulty

$$m_{fk}(t,t') = -i\left\langle T_K\left[c_{fk}^{\dagger}(t) + c_{fk}(t)\right]\left[c_{fk}^{\dagger}(t') - c_{fk}(t')\right]\right\rangle. \tag{13}$$

Indeed, its retarded, advanced, and Keldysh components are $\overline{m_f^{R,A}(\omega)} = 0$, and

$$\begin{aligned} \overline{m_f^K(\omega)} &= (2i/v_F)\sum_n J_n^2\left(\frac{V_{ac}}{\Omega}\right) \\ &\quad \times \left\{f\left(\omega - n\Omega + V_{dc}\right) - f\left(\omega + n\Omega - V_{dc}\right)\right\}. \end{aligned} \tag{14}$$

3.2 Interacting Majorana Green's functions

In order to compute physical quantities, it is necessary to calculate the advanced, retarded, and Keldysh components of the Majorana Green's functions, which are defined as:

$$G_{\alpha\beta}(t,t') = -i\left\langle T_K\left\{\alpha(t)\,\beta(t')\right\}\right\rangle,\ \alpha,\beta = \hat{a},\hat{b}. \tag{15}$$

The Green's functions $G_{aa}^A(t,t')$ are used to calculate the differential conductance, whereas the Keldysh Green's function $G_{ba}^K(t,t')$ is used to calculate the magnetic susceptibility.

Using the interaction representation, we rewrite the Green's functions by invoking the S matrix, with the assumption of coupling parameters $J_i(t)$ in equation (6). We obtain the advanced Green's functions

$$\begin{aligned} G_{ba}^A(t,t') &= -H\int_{-\infty}^{\infty} dt_1\Theta(t_1-t)G_{aa}^A(t_1,t') \\ &\quad - \int_{-\infty}^{\infty} dt_1\Gamma_s(t_1)\,\Theta(t_1-t)G_{ba}^A(t_1,t'), \\ G_{aa}^A(t,t') &= i\Theta(t'-t) + H\int_{-\infty}^{\infty} dt_1\Theta(t_1-t)G_{ba}^A(t_1,t') \\ &\quad - \int_{-\infty}^{\infty} dt_1\Gamma_{at}(t_1)\,\Theta(t_1-t)G_{aa}^A(t_1,t'), \end{aligned} \tag{16}$$

where

$$\begin{aligned} \Gamma_s(t) &= \Gamma_{s0} + 2\sqrt{\Gamma_{s0}\Gamma_s}\cos(\Omega_1 t) + \Gamma_s\cos^2(\Omega_1 t), \\ \Gamma_{at}(t) &= \Gamma_{at}\cos^2(\Omega_1 t). \end{aligned} \tag{17}$$

Here we have defined $\Gamma_t = (J_{\perp}^{RL})^2/4\pi a v_F$, $\Gamma_a = (J_{\perp}^{LL} - J_{\perp}^{RR})^2/16\pi a v_F$, $\Gamma_{at} = \Gamma_t + \Gamma_a$, $\Gamma_{s0} = (J_{\perp 0}^{LL} + J_{\perp 0}^{RR})^2/16\pi a v_F$, $\Gamma_s = (J_{\perp}^{LL} + J_{\perp}^{RR})^2/16\pi a v_F$. Equation (16) induces the Schiller-Hershfield results when all couplings are time independent. One can easily take the Fourier transform of equation (16), and then obtain again the exact formulas of the advanced Majorana Green's functions, which were previously obtained [15].

In order to find the Green's function $G^A_{aa}(t,t')$, we first change equation (16) to differential equations by taking the derivative with respect to time t. We obtain

$$\begin{aligned}&[\partial_t - \Gamma_s(t)]\, G^A_{ba}(t,t') = H G^A_{aa}(t,t'),\\ &[\partial_t - \Gamma_{at}(t)]\, G^A_{aa}(t,t') + H G^A_{ba}(t,t') = -i\delta(t-t'). \end{aligned} \quad (18)$$

We define the non-interacting Green's functions $g^A_{at/s}(t,t')$ as [38]

$$\left[\partial_t - \Gamma_{at/s}(t)\right] g^A_{at/s}(t,t') = \delta(t-t'), \quad (19)$$

so

$$\begin{aligned} g^A_{at}(t,t') =& -\Theta(t'-t)\exp\left[\frac{\Gamma_{at}}{2}(t-t')\right]\\ &\times\exp\left[\frac{\Gamma_{at}}{4\Omega_1}\left[\sin(2\Omega_1 t)-\sin(2\Omega_1 t')\right]\right],\\ g^A_s(t,t') =& -\Theta(t'-t)\exp\left[\left(\Gamma_{s0}+\frac{\Gamma_s}{2}\right)(t-t')\right]\\ &\times\exp\left[\frac{2\sqrt{\Gamma_{s0}\Gamma_s}}{\Omega_1}\left[\sin(\Omega_1 t)-\sin(\Omega_1 t')\right]\right]\\ &\times\exp\left[\frac{\Gamma_s}{4\Omega_1}\left[\sin(2\Omega_1 t)-\sin(2\Omega_1 t')\right]\right]. \end{aligned} \quad (20)$$

From equations (18) and (19), we obtain

$$\int_{-\infty}^{\infty} dt_1 \left[\left[g^A_{at}(t,t_1)\right]^{-1} + H^2 g^A_s(t,t_1)\right] G^A_{aa}(t_1,t') = -i\delta(t-t'). \quad (21)$$

One can see that the non-interacting Green's functions $g^A_{at/s}(t,t')$ always oscillate on time with frequency $\Omega_1 = \Omega/p$. Therefore any cut-off for the boundary of the integrals in equation (21) may result in serious shortcomings. However, after changing time variables as in equation (9), $g^A_{at/s}(t,t')$ oscillates around smooth averaging functions $\overline{g^A_{at/s}(\tau,T)}$ with $T \gg \Omega_1^{-1}$. Hence, we adopt an approximation by averaging the Green's functions over time T in a period of $2\pi/\Omega_1$. We then rewrite them in Fourier space as:

$$\overline{g^A_{at}(\omega)} = \sum_{n=-\infty}^{\infty} J_n^2\left(-i\frac{\Gamma_{at}}{4\Omega_1}\right)\frac{i}{\omega+2n\Omega_1 - i\frac{\Gamma_{at}}{2}}, \quad (22)$$

and

$$\begin{aligned}\overline{g^A_s(\omega)} =& \sum_{m,n,k=-\infty}^{\infty} J_{m-2n+2k}\left(-i\frac{2\sqrt{\Gamma_{s0}\Gamma_s}}{\Omega_1}\right)\\ &\times J_m\left(-i\frac{2\sqrt{\Gamma_{s0}\Gamma_s}}{\Omega_1}\right) J_n\left(-i\frac{\Gamma_s}{4\Omega_1}\right) J_k\left(-i\frac{\Gamma_s}{4\Omega_1}\right)\\ &\times\frac{i}{\omega+(m+2k)\Omega_1 - i\left(\Gamma_{s0}+\frac{\Gamma_s}{2}\right)}. \end{aligned} \quad (23)$$

Thus we obtain

$$\overline{G^A_{aa}(\omega)} = \frac{-i}{\overline{g^A_{at}(\omega)}^{-1} + H^2\overline{g^A_s(\omega)}}. \quad (24)$$

The meaning of the averaging method is that we have smoothed the fine oscillations of the Green's functions. It works well in the high frequency regime, namely, $T \gg \Omega_1^{-1}$, but not too high in order to neglect the charge fluctuations on the dot. In fact, as we discuss later, the method works well in the regime $\hbar\Omega \gtrsim k_B T_K$. It offers the opportunity to compute the physical observables non-perturbatively. The results obtained by the averaging method should be close to the exact solution while the results from the perturbation calculation cannot be. However, the averaging method cannot be applied for the adiabatic limit. The adiabatic regime should be considered separately [39]. In the next section, we calculate the differential conductance and magnetic impurity susceptibility by using this averaging method.

4 Average physical observables

In this section we will compute average differential conductance and magnetic susceptibility, and discuss the results.

4.1 Average charge current and average differential conductance

First, we are interested in calculating the time averaged charge current through the junction I_c. The time averaged differential conductance $G = dI_c/dV_{dc}$ is accessible experimentally. We compute it by using the Keldysh nonequilibrium Green's function technique. The current at a time t is expressed as:

$$I_c(t) = -(eJ_t(t)/8\pi a)\Re\int_{-\infty}^{\infty} dt_1 J_t(t_1) m^K_f(t,t_1) G^A_{aa}(t_1,t).$$

The Majorana Green's functions $G^A_{aa}(t_1,t)$ are calculated averagely in the above section with its Fourier transformation is shown in equation (24). After the averaging procedure over time T, the average current at a time t is written as:

$$\begin{aligned}\overline{I_c(t)} =& \frac{J_t(t)}{16\pi^3 a v_F}\Im\int_{-\infty}^{\infty} dt_1 J_t(t_1)\int_{-\infty}^{\infty} d\omega\int_{-\infty}^{\infty} d\omega_1 \sum_n J_n^2\left(\frac{V_{ac}}{\Omega}\right)\\ &\times\left[f(\omega+n\Omega-V_{dc}) - f(\omega-n\Omega+V_{dc})\right]\\ &\times e^{-i\omega(t-t_1)}\overline{G^A_{aa}(\omega_1)} e^{-i\omega_1(t_1-t)}. \end{aligned} \quad (25)$$

As discussed above, the current should oscillate on time with period $2\pi\Omega_1^{-1}$. It is possible to take the average of the current over time t in a period of $2\pi p\Omega^{-1}$. So the average

current is:

$$\begin{aligned}\overline{I_c} &= \frac{\Omega}{2\pi p}\int_0^{2\pi p/\Omega} dt\overline{I_c(t)} \\ &= \frac{\Gamma_t}{8\pi}\Im\int_{-\infty}^{\infty}d\omega\sum_n J_n^2\left(\frac{V_{ac}}{\Omega}\right) \\ &\times\Big\{\left[f\left(\omega+(n-1/p)\,\Omega-V_{dc}\right)-f\left(\omega-(n+1/p)\right.\right. \\ &\times\Omega+V_{dc}\big)+f\left(\omega+(n+1/p)\,\Omega-V_{dc}\right) \\ &-f\left(\omega-(n-1/p)\,\Omega+V_{dc}\right)\big]\overline{G_{aa}^A(\omega)}\Big\}. \end{aligned} \tag{26}$$

Here, we have averaged the Majorana Green's function over the period of $2\pi p\Omega^{-1}$. This averaging procedure has smoothed the Majorana Green's function, and only kept the absorption or emission of one mode generated by the ac couplings. The other modes already present in the averaged Majorana Green's function in equations (22)–(24), and contribute to the average current indirectly. Instead of the time-dependent current, the average current in equation (26) is usually used to calculate the differential conductance [26]

$$\overline{G} = \frac{d\overline{I_c}}{dV_{dc}} = \frac{d\left[\frac{\Omega}{2\pi p}\int_0^{2\pi p/\Omega} I_c(t)\,dt\right]}{dV_{dc}}. \tag{27}$$

The conductance and the magnetic susceptibility behaviors remain when the temperature is varied from absolute zero to a small temperature. If the temperature is kept increasing much below the Kondo temperature, the conductance and the susceptibility behaviors are broadened and then smeared. For convenient computation, we consider the time averaged differential conductance at the absolute zero

$$\begin{aligned}\overline{G} = \frac{\Gamma_t}{8\pi}\Im\sum_{n=-\infty}^{\infty} J_n^2\left(\frac{V_{ac}}{\Omega}\right)\Big\{&\overline{G_{aa}^A\left(V_{dc}-(n-1/p)\,\Omega\right)} \\ &+\overline{G_{aa}^A\left(-V_{dc}+(n+1/p)\,\Omega\right)}+\overline{G_{aa}^A\left(V_{dc}-(n+1/p)\,\Omega\right)} \\ &+\overline{G_{aa}^A\left(-V_{dc}+(n-1/p)\,\Omega\right)}\Big\}. \end{aligned} \tag{28}$$

We will discuss the behavior of the average differential conductance as a function of magnetic field and source-drain voltage.

4.2 Average impurity magnetization and susceptibility

In addition to the tunneling conductance, the magnetic susceptibility is also a physical quantity observed by experiments. It is a response of the system to an external magnetic field coupled to the impurity spin. The magnetic susceptibility is the derivative of the magnetization, which can be calculated from the following formula

$$M(H) = \frac{\mu_B g_i}{4\pi}\int_{-\infty}^{\infty} d\omega G_{ba}^K(\omega). \tag{29}$$

The Majorana Green's function $G_{ba}^K(\omega)$ is calculated averagely in the same way as we have calculated for $G_{aa}^A(\omega)$. The magnetization is understood as the "average" one and is expressed as:

$$M(H) = \frac{(\mu_B g_i)\,H}{4\pi}\int_{-\infty}^{\infty} d\omega\frac{\overline{g_s^K(\omega)}\left[\overline{g_{at}^K(\omega)}\overline{\Lambda_{at}(\omega)}+\overline{\Lambda_s(\omega)}\right]}{1+H^2\overline{g_{at}^K(\omega)}\overline{g_s^K(\omega)}}, \tag{30}$$

where the average non-interacting Green's functions

$$\overline{g_{at}^K(\omega)} = \sum_{n=-\infty}^{\infty} J_n^2\left(i\frac{\Gamma_{at}}{4\Omega_1}\right)\frac{i}{\omega+2n\Omega_1+i\frac{\Gamma_{at}}{2}}, \tag{31}$$

$$\begin{aligned}\overline{g_s^K(\omega)} = \sum_{m,n,k=-\infty}^{\infty} &J_{m-2n+2k}\left(i\frac{2\sqrt{\Gamma_{s0}\Gamma_s}}{\Omega_1}\right) \\ &\times J_m\left(i\frac{2\sqrt{\Gamma_{s0}\Gamma_s}}{\Omega_1}\right)J_n\left(i\frac{\Gamma_s}{4\Omega_1}\right)J_k\left(i\frac{\Gamma_s}{4\Omega_1}\right) \\ &\times\frac{i}{\omega+(m+2k)\,\Omega_1+i\left(\Gamma_{s0}+\frac{\Gamma_s}{2}\right)}, \end{aligned} \tag{32}$$

and the average $\overline{\Lambda_{at/s}(\omega)}$ are:

$$\begin{aligned}\overline{\Lambda_{at}(\omega)} = \overline{G_{aa}^A(\omega)}\Big\{&\Gamma_a\left[f(\omega-\Omega/p)+f(\omega+\Omega/p)-1\right] \\ &+\frac{\Gamma_t}{2}\sum_n J_n^2\left(\frac{V_{ac}}{\Omega}\right)\big[f(\omega-(n+1/p)\Omega+V_{dc}) \\ &+f(\omega+(n-1/p)\Omega-V_{dc})+f(\omega-(n-1/p) \\ &\times\Omega+V_{dc})+f(\omega+(n+1/p)\Omega-V_{dc})-2\big]\Big\}, \end{aligned} \tag{33}$$

$$\begin{aligned}\overline{\Lambda_s(\omega)} = \overline{g_s^A(\omega)}\,\overline{G_{aa}^A(\omega)}\Big\{&2\Gamma_{s0}\left[2f(\omega)-1\right] \\ &+\Gamma_s\left[f(\omega-\Omega/p)+f(\omega+\Omega/p)-1\right]\Big\}. \end{aligned} \tag{34}$$

From equation (30), when the system is applied either a constant voltage bias $V_{sd}=V_{dc}$ or a time dependent one $V_{sd}=V_{dc}+V_{ac}\cos(\Omega t)$ and the Kondo couplings are time independent, again, we recover the results of the Schiller-Hershfield theory [15,18].

5 Results and discussions

In this section we present typical results of the tunneling conductance and the magnetic susceptibility. In all plots, the horizontal axis is the magnetic energy $H=\mu_B g_i B$, B is the amplitude of the applied magnetic field, the vertical axis is either the tunneling conductance $G/(e^2/\hbar)$ or the magnetic susceptibility $\chi/(g_i\mu_B)^2$. We choose $\Gamma_{s0}=1$ as the energy scale. We find that the results obtained at very small temperature and at absolute zero are similar. For convenience, we calculate the tunneling conductance at absolute zero and the magnetic susceptibility at very small temperature ($T=0.05$).

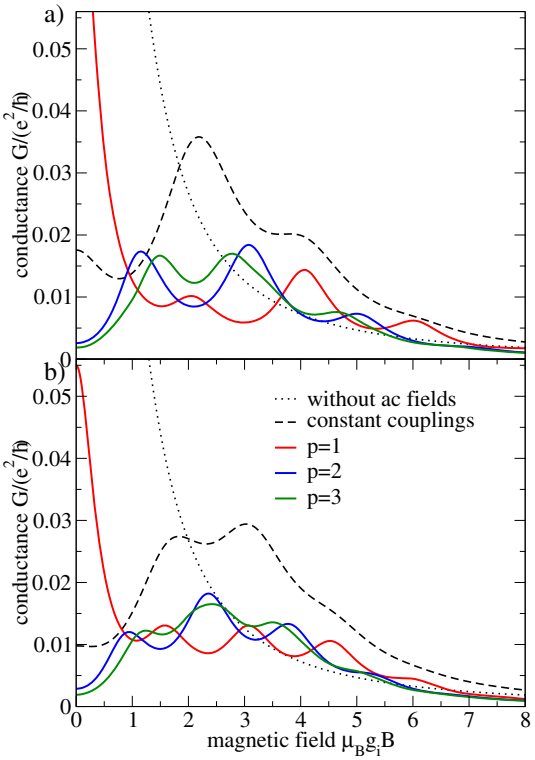

Fig. 1. The magnetic field dependence of the conductance $G(H)$ for $V_{ac} = 4$, $\Gamma_{at} = 0.3$, $\Gamma_s = 0.05$, $\Gamma_t = 0.25$, $V_{dc} = 0$, and (a) $\hbar\Omega = 2$ and (b) $\hbar\Omega = 1.5$. The dotted black line is the conductance without the harmonic time-dependent fields; the Kondo peak is at $\mu_B g_i B = 0$. The dashed black line is the conductance with the harmonic time-dependent voltage only, the constant couplings are: $J_\perp^{\alpha\beta} = J_{\perp 0}^{\alpha\beta} + J_{\perp 1}^{\alpha\beta}$; the Kondo satellites peak at $\mu_B g_i B = n\hbar\Omega$; the highest peak's position depends on $eV_{ac}/\hbar\Omega$. When both voltage and couplings are oscillating in time, the peaks occur at $\mu_B g_i B = (n \pm 1/p)\,\hbar\Omega$; the solid red, blue, green lines are the conductance for the $p = 1, 2, 3$, respectively. The peak splitting due to the time-dependent couplings can be seen at the highest peak.

In Figures 1 and 3, the conductance G and the susceptibility χ are plotted as functions of magnetic field H for different cases: in the absence of the ac fields (dotted black curves), with only time-dependent voltage (the couplings are time independent) (dashed black curves), and in the presence of both time-dependent voltage and couplings with various values of p (red, blue, and green lines for $p = 1$, $p = 2$, and $p = 3$, respectively). As we have discussed in Section 2, when the time-dependent parts of the couplings vanish, the two leads are decoupled and there is no tunneling current. However, when the couplings are time independent, in addition to these time-independent couplings we include also the finite amplitude constants $J_{\lambda 1}^{\alpha\beta}$ (without the oscillation parts), there is a tunneling current through the dot. This case is referred as the constant couplings in these figures. Figure 1 shows that the conductance is strongly reduced when the couplings are time independent. The satellites appear at $\mu_B g_i B = eV_{dc} \pm n\hbar\Omega$ $(n \in \mathbb{Z})$ due to the oscillation of source-drain voltage $V_{ac}(t)$ [16,18–26]. However, the satellites only appear when $eV_{ac}/\hbar\Omega$ is big enough compare to 1 (but $eV_{ac} \sim \hbar\Omega$, as well as $\hbar\Omega \sim k_B T_K$ and $\hbar\Omega > k_B T_K$ in order to avoid decoherences), and this ratio determines the height of side-band peaks. For instance, in Figure 1a plotted for $1 < eV_{ac}/\hbar\Omega \leq 2$, the highest peak is at $\mu_B g_i B = \hbar\Omega$ besides the trivial main peak at $\mu_B g_i B = 0$. The strength of the ac fields is small compared to the strength of the magnetic field, which reduces strongly the Kondo conductance. When the oscillation amplitude increases, it is dominant over the magnetic field, and reduces strongly the peak at $\mu_B g_i B = 0$, while at the same time it increases the satellite peak at $\mu_B g_i B = 2\hbar\Omega$ as shown in Figure 1b for $eV_{ac}/\hbar\Omega > 2$. One can say that the highest satellite peak position depends on the ratio $eV_{ac}/\hbar\Omega$. However, it is impossible to see the highest satellite peak at high magnetic fields, for instance at $\mu_B g_i B = 3\hbar\Omega$, due to the strong suppression of the satellite peaks by both magnetic field and voltage.

We now discuss the effect of the ac Kondo couplings. In fact, the oscillation of Kondo couplings comes from the oscillation of the gate voltage of a QD. It can be considered as an indirect effect. In Figure 1, one can see that when the couplings oscillate with frequency $\Omega_1 = \Omega/p$ with $p \in \mathbb{N}$, each main satellite peak splits into two peaks. When a peak is split into two peaks, the height of these two peaks relate to the height of original peak. The distance between an original peak and its split peak is $d_{peak} = \hbar\Omega/p$. This can be understood by investigating the Green's function $G_{aa}^A(\omega)$. The difference between the coupling frequency and the voltage frequency is described by an integer number $p \geq 1$. However, p cannot be too big because the slow oscillation in couplings can be considered as constant compared to the fast oscillation of voltage. When $p = 1$, the couplings oscillate on time with the same frequency as the voltage, the satellite peaks split into two peaks with the distance $d_{peak} = \hbar\Omega$ equal to the satellite peak distance. Thus, for $p = 1$, the peaks remain but their height changes drastically due to the re-contribution of energy through the peak splitting. This peak splitting effect can be seen clearly if $p = 2$, or $p = 3$. As we have explained the number p can also be bigger than 1. The peak splitting can be seen clearly at the highest satellite peak. When we increase p the splitting distance d_{peak} decreases, the splitting becomes weak then approaches the limit in which the couplings are constant. This result implies a possibility that one sees peaks appearing at a distance $\mu_B g_i B < \hbar\Omega$ in the regime of weak magnetic field. We predict p is a frequency dependent systematic parameter. For the case $p = 1$, we can check the height of the satellite peaks to confirm the oscillations on voltage and couplings.

Besides, from Figure 2, we find that the main characteristic of $G(H)$ lightly depends on scales Γ_i, $(i = at, s, t)$. Γ_i are chosen much smaller than Γ_{s0} because the ac parts in the couplings should be small compared to the existing dc parts. We vary each energy scale Γ_s, Γ_{at}, Γ_t, while the other parameters are fixed. $\Gamma_t \sim \left(J_\perp^{LR}\right)^2$ concerns the coupling between two leads and it controls the spin-flip tunneling of electrons through QD. $\Gamma_s \sim \left[J_\perp^{LL} + J_\perp^{RR}\right]^2$

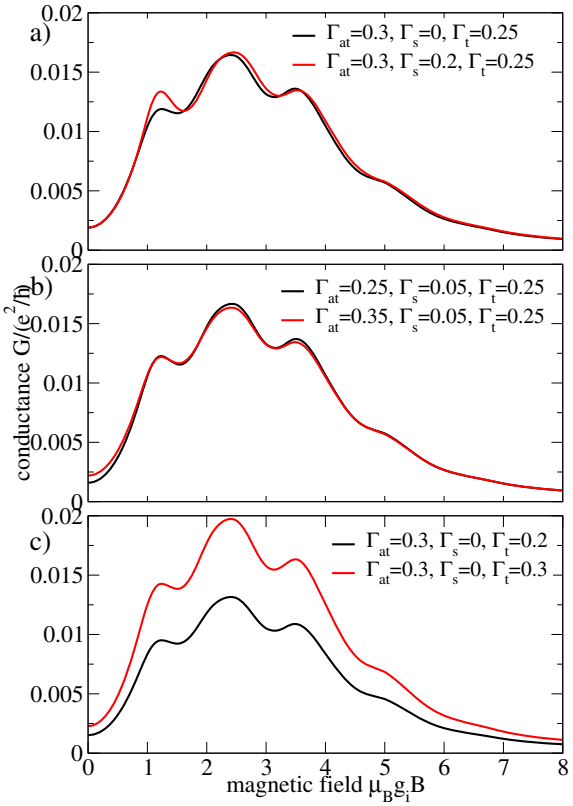

Fig. 2. The magnetic field dependence of the conductance $G(H)$ for $V_{ac} = 4$, $\hbar\Omega = 1.5, p = 3$, $V_{dc} = 0$. The other model parameters are indicated in the plots. Notice that the conductance amplitude strongly depends on Γ_t.

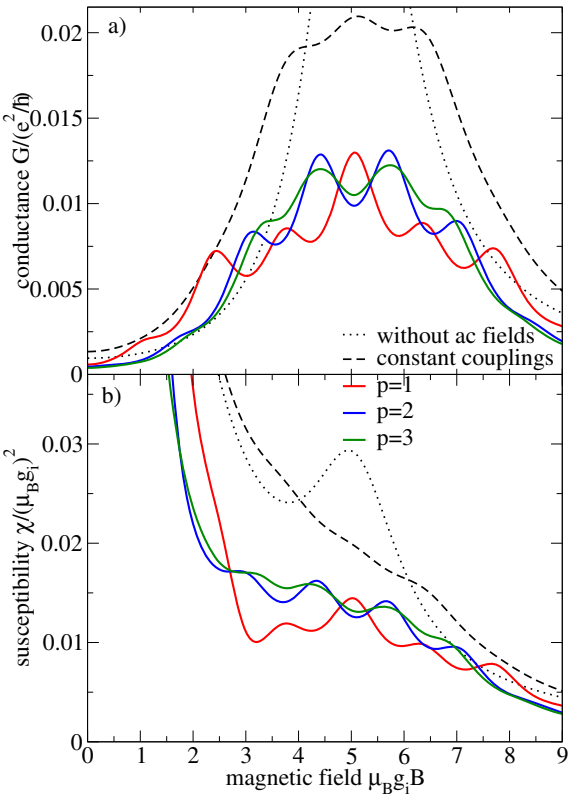

Fig. 3. The conductance $G(H)$ (a) and the susceptibility $\chi(H)$ (b) as a function of the magnetic field for $\hbar\Omega = 1.35$, $eV_{ac} = 2$, $V_{dc} = 5$, $\Gamma_{at} = 0.3$, $\Gamma_s = 0.1$, $\Gamma_t = 0.25$. The dotted black line is the results without the harmonic time-dependent fields; the Kondo peak is at $\mu_B g_i B = eV_{dc}$. The dashed black line is the results with the harmonic time-dependent voltage only, the constant couplings are: the Kondo satellites peak at $\mu_B g_i B = eV_{dc} \pm n\hbar\Omega$. When both the voltage and the Kondo couplings are oscillating in time, the peaks occur at $\mu_B g_i B = eV_{dc} \pm (n \pm 1/p)\,\hbar\Omega$; the solid red, blue, green curves are the results for the $p = 1$, 2, 3, respectively.

concerns the sum of separated couplings in each lead and is small compared to Γ_{s0}. $\left(J_\perp^{LL} - J_\perp^{RR}\right)^2$ contributes to Γ_{at}. Both energy scales Γ_{at} and Γ_s affect slightly the $G(H)$ behavior. Figure 2c shows that the amplitude of conductance strongly decreases with decreasing Γ_t. It vanishes when $\Gamma_t = 0$. Thus, any small oscillation in the transverse couplings drives the system away from the uncoupled isotropic two-channel Kondo situation.

In Figure 3, the magnetic susceptibility is plotted as a function of magnetic field at temperature $T = 0.05$. As previously found from $G(H)$ characteristic, dc voltage V_{dc} also splits the satellite peaks [16] when it is smaller than the ac voltage V_{ac}. The fact that V_{dc} splits peaks by a distance $\pm eV_{dc}$ is understood in non-equilibrium dc Kondo physics of a QD [15]. Significantly, if V_{dc} is bigger than V_{ac}, we see the peak splitting due to the oscillations of couplings. If $V_{dc} = 0$, we see the satellite peaks dominate at $\mu_B g_i B = 0$. The other peaks at $\mu_B g_i B = k\hbar\Omega$ ($k = \pm 1, \pm 2, \ldots$) are very weak. To study the satellite peak splitting due to the coupling oscillation, we choose $V_{dc} > V_{ac}$. We find that all susceptibility-magnetic field and conductance-magnetic field characteristics are the same. It is evident that the relation between susceptibility and conductance shown in formula (8.9) of reference [15] can be generalized when the system is in the ac fields.

The differential conductance G and magnetic susceptibility χ are also plotted as functions of dc voltage V_{dc} in Figures 4 and 5. In order to investigate the effect of the ac fields, we consider the case in which no magnetic field is applied. Again, we find the two-fold peak splitting (i.e., the Kondo satellite splitting) due to both voltage and Kondo coupling oscillations. There is more challenge to determine it in the cases $p = 1$ and $p = 2$. The distance between peaks is still $\hbar\Omega$. For $p = 1$, the positions of peaks are the same as those in the case when only voltage oscillates, but the peak heights are re-contributed. For $p = 2$, both the positions and heights of peaks are re-contributed, satellite peaks are shifted by $\hbar\Omega/2$. For $p \geq 3$, our interesting results show that one has a chance to see two peaks, whose distance is much smaller than $\hbar\Omega$. For instance, as shown in Figures 4 and 5, when $p = 3$, two peaks are split from a satellite peak at a distance of $2\hbar\Omega/3$. Moreover, one can also additionally find two peaks at a distance of $\hbar\Omega/3$. They are the peaks that are split from the consecutive satellite peaks.

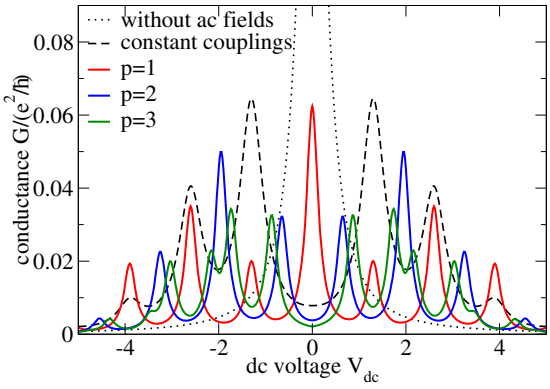

Fig. 4. The conductance $G(V_{dc})$ as a function of the constant voltage V_{dc} for $\hbar\Omega = 1.3$, $eV_{ac} = 3$, $\Gamma_{at} = 0.3$, $\Gamma_s = 0.05$, $\Gamma_t = 0.2$, $H = 0$. The dotted black line is the conductance without the harmonic time-dependent fields; the Kondo peak is at $eV_{dc} = 0$. The dashed black line is the conductance with the harmonic time-dependent voltage only; the Kondo satellites are at $eV_{dc} = \pm n\hbar\Omega$. When both the voltage and the Kondo couplings are oscillating in time, the peaks occur at $eV_{dc} = \pm(n \pm 1/p)\hbar\Omega$; the solid red, blue, green lines are the conductance for the $p = 1, 2, 3$, respectively.

6 Conclusions

In this paper, we have investigated the satellite splitting due to the ac fields in the non-equilibrium Kondo model at the Toulouse limit. Both the oscillations in the source-drain voltage and in the Kondo couplings are investigated. The bosonization technique and the non-equilibrium Green's function method are employed. We have proposed a non-perturbative approximation, in which we have smoothed the fine fast oscillations around its average form. Thus, the Green's functions and the observables are averaged. Our averaging method works well for the cases $\hbar\Omega \gtrsim k_B T_K \sim \Gamma_{s0} \gg \Gamma_{at/s/t}$ but $\hbar\Omega \ll |E_d|, |U - E_d|$ in which the external fields do not ionize the dot and/or induce charge fluctuations on it.

The center result of our work is the satellite peak splitting. This feature occurs when the oscillation parts are added to the Kondo couplings. The distance between two peaks, which are split from a satellite, is $2\hbar\Omega/p$, the distance between two peaks, which are split from two consecutive satellites, is $(p-1)\hbar\Omega/p$, while the distance between two satellites is $\hbar\Omega$. All the satellite splitting distances depend on the number p, which describes the difference between the frequency of the Kondo couplings and the frequency of the voltage. We find the two close peaks clearly at small magnetic field in $G(H), \chi(H)$ characteristics and small dc voltage in $G(V_{dc}), \chi(V_{dc})$ characteristics.

Magnetic field and applied dc and ac voltages suppress the Kondo correlation, alternatively. When an ac source-drain voltage is applied, the Kondo peak is expanded into satellites with $d_{peak} = n\hbar\Omega$ [16,18–25]. When all above external fields are applied to a QD system, the equilibrium Kondo peak is split into satellites. The position of a satellite is determined based on the relation: $\mu_B g_i B = \pm eV_{dc} \pm (n \pm 1/p)\hbar\Omega$ if the Kondo couplings

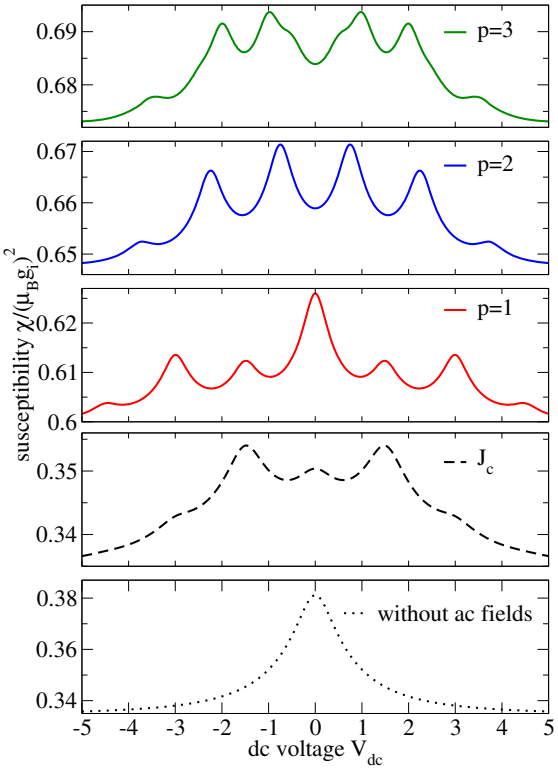

Fig. 5. The magnetic susceptibility $\chi(V_{dc})$ as a function of the constant voltage V_{dc} for $\hbar\Omega = 1.5$, $eV_{ac} = 2.5$, $\Gamma_{at} = 0.3$, $\Gamma_s = 0.1$, $\Gamma_t = 0.25$, $H = 0$. The dotted black line is the susceptibility without the harmonic time-dependent fields; the Kondo peak is at $eV_{dc} = 0$. The dashed black line is the susceptibility with the harmonic time-dependent voltage only; the Kondo satellites are at $eV_{dc} = \pm n\hbar\Omega$. When both the voltage and the Kondo couplings are oscillating in time, the satellites peaks occur at $eV_{dc} = \pm(n \pm 1/p)\hbar\Omega$; the solid red, blue, green lines are the susceptibility for the $p = 1, 2, 3$, respectively.

are considered oscillating on time with frequency $\hbar\Omega/p$. However, so far we have shown the satellite splitting only at the Toulouse limit, but it is also expected away from the Toulouse limit. It is worth to investigate the time-dependent the Kondo model away from the Toulouse limit.

We acknowledge Carlos Bolech, Nayana Shah, Andrei Kogan, Bryan Hemingway, Philippe Dollfus, and Mikhail Kiselev for the usefull discussions. T.T.K.N. is supported by University of Cincinnati and the National Foundation for Science and Technology Development (NAFOSTED) of Vietnam (No. 103.02-2012.52).

References

1. J. Kondo, Prog. Theor. Phys. **32**, 37 (1964)
2. A.C. Hewson, *The Kondo Problem to Heavy Fermions, Cambridge Studies in Magnetism* (Cambridge University Press, Cambridge, 1993)
3. L.I. Glazman, M.E. Raikh, Pis'ma Zh. Eksp. Teor. Fiz. **47**, 378 (1988) [J. Exp. Theor. Phys. Lett. **47**, 453 (1988)]

4. T.K. Ng, P.A. Lee, Phys. Rev. Lett. **61**, 1768 (1988)
5. S. Hershfield, J.H. Davies, J.W. Wilkins, Phys. Rev. Lett. **67**, 3720 (1991)
6. D. Goldhaber-Gordon, H. Shtrikman, D. Mahalu, D. Abusch-Magder, U. Meirav, M.A. Kastner, Nature **391**, 156 (1998)
7. S.M. Cronenwett, T.H. Oosterkamp, L.P. Kouwenhoven, Science **281**, 540 (1998)
8. J. Schmid, J. Weis, K. Eberl, K. von Klitzing, Physica B **256**, 182 (1998)
9. Y. Meir, N.S. Wingreen, P.A. Lee, Phys. Rev. Lett. **70**, 2601 (1993)
10. T.K. Ng, Phys. Rev. Lett. **70**, 3635 (1993)
11. M.H. Hettler, J. Kroha, S. Hershfield, Phys. Rev. Lett. **73**, 1967 (1994)
12. M. Pustilnik, L. Glazman, J. Phys.: Condens. Matter **16**, R513 (2004)
13. M. Grobis, I.G. Rau, R.M. Potok, D. Goldhaber-Gordon, The Kondo Effect in Mesoscopic Quantum Dots, in *Handbook of Magnetism and Advanced Magnetic Materials*, edited by H. Kronmüller, S. Parkin (Wiley, 2007)
14. A. Schiller, S. Hershfield, Phys. Rev. B **51**, 12896 (1995)
15. A. Schiller, S. Hershfield, Phys. Rev. B **58**, 14978 (1998)
16. M.H. Hettler, H. Schoeller, Phys. Rev. Lett. **74**, 4907 (1995)
17. T.K. Ng, Phys. Rev. Lett. **76**, 487 (1996)
18. A. Schiller, S. Hershfield, Phys. Rev. Lett. **77**, 1821 (1996)
19. Y. Goldin, Y. Avishai, Phys. Rev. Lett. **81**, 5394 (1998)
20. Y. Goldin, Y. Avishai, Phys. Rev. B **61**, 16750 (2000)
21. R. Lopez, R. Aguado, G. Platero, C. Tejedor, Phys. Rev. Lett. **81**, 4688 (1998)
22. R. Lopez, R. Aguado, G. Platero, C. Tejedor, Phys. Rev. B **64**, 075319 (2001)
23. A. Kaminski, Yu.V. Nazarov, L.I. Glazman, Phys. Rev. Lett. **83**, 384 (1999)
24. A. Kaminski, Yu.V. Nazarov, L.I. Glazman, Phys. Rev. B **62**, 8154 (2000)
25. P. Nordlander, N.S. Wingreen, Y. Meir, D.C. Langreth, Phys. Rev. B **61**, 2146 (2000)
26. A. Kogan, S. Amasha, M.A. Kastner, Science **304**, 1293 (2004)
27. P.K. Tien, J.P. Gordon, Phys. Rev. **129**, 647 (1963)
28. G. Toulouse, C.R. Acad. Sci. Paris **268**, 1200 (1969)
29. V.J. Emery, S. Kivelson, Phys. Rev. B **46**, 10812 (1992)
30. D. Lobaskin, S. Kehrein, Phys. Rev. B **71**, 193303 (2005)
31. C. Tomaras, S. Kehrein, Europhys. Lett. **93**, 47011 (2011)
32. M. Heyl, S. Kehrein, Phys. Rev. B **81**, 144301 (2010)
33. J.R. Schrieffer, P.A. Wolff, Phys. Rev. **149**, 491 (1966)
34. T. Giamarchi, *Quantum Physics in One Dimension* (Oxford University Press, New York, 2004)
35. A.M. Zagoskin, Quantum Theory of Many-Body Systems: Techniques and Applications, in series *Graduate Texts in Contemporary Physics* (Springer-Verlag, Berlin and Heidelberg, 1998)
36. A.-P. Jauho, N.S. Wingreen, Y. Meir, Phys. Rev. B **50**, 5528 (1994)
37. O.A. Tretiakov, A. Mitra, Phys. Rev. B **81**, 024416 (2010)
38. M.T. Tran, Phys. Rev. B **78**, 125103 (2008)
39. A. Schiller, A. Silva, Phys. Rev. B **77**, 045330 (2008)